Biochimica et Biophysica Acta 1797 (2010) 1617–1626

Contents lists available at ScienceDirect

Biochimica et Biophysica Acta

journal homepage: www.elsevier.com/locate/bbabio

Electronic structure of the primary electron donor of *Blastochloris viridis* heterodimer mutants: High-field EPR study

N.S. Ponomarenko [a,1], O.G. Poluektov [b,*], E.J. Bylina [a,2], J.R. Norris [a]

[a] Department of Chemistry, University of Chicago, 929 E. 57th Street, GCIS, Chicago, IL 60637, USA
[b] Chemical Sciences and Engineering Division, Argonne National Laboratory, 9700 S. Cass Avenue, Argonne, IL 60439, USA

ARTICLE INFO

Article history:
Received 21 September 2009
Received in revised form 18 May 2010
Accepted 4 June 2010
Available online 11 June 2010

Keywords:
Blastochloris viridis
Heterodimer mutant
High-field EPR
Triplet state
Heterodimer
Photosynthetic reaction center
Cytochrome
Electron transfer

ABSTRACT

High-field electron paramagnetic resonance (HF EPR) has been employed to investigate the primary electron donor electronic structure of *Blastochloris viridis* heterodimer mutant reaction centers (RCs). In these mutants the amino acid substitution His(M200)Leu or His(L173)Leu eliminates a ligand to the primary electron donor, resulting in the loss of a magnesium in one of the constituent bacteriochlorophylls (BChl). Thus, the native BChl/BChl homodimer primary donor is converted into a BChl/bacteriopheophytin (BPhe) heterodimer. The heterodimer primary donor radical in chemically oxidized RCs exhibits a broadened EPR line indicating a highly asymmetric distribution of the unpaired electron over both dimer constituents. Observed triplet state EPR signals confirm localization of the excitation on the BChl half of the heterodimer primary donor. Theoretical simulation of the triplet EPR lineshapes clearly shows that, in the case of mutants, triplet states are formed by an intersystem crossing mechanism in contrast to the radical pair mechanism in wild type RCs. Photooxidation of the mutant RCs results in formation of a BPhe anion radical within the heterodimer pair. The accumulation of an intradimer BPhe anion is caused by the substantial loss of interaction between constituents of the heterodimer primary donor along with an increase in the reduction potential of the heterodimer primary donor D/D^+ couple. This allows oxidation of the cytochrome even at cryogenic temperatures and reduction of each constituent of the heterodimer primary donor individually. Despite a low yield of primary donor radicals, the enhancement of the semiquinone–iron pair EPR signals in these mutants indicates the presence of kinetically viable electron donors.

Published by Elsevier B.V.

1. Introduction

The key step of solar energy conversion in natural photosynthetic systems involves rapid light-induced sequential electron transfer (ET) in the reaction center (RC) protein complexes resulting in efficient charge separation across a biological membrane [1,2]. The first insights into the function and structure of photosynthetic RCs were facilitated to a considerable extent by biochemical and spectroscopic investigations [3]. One of the unique structural attributes of RCs revealed by spectroscopic methods is the dimeric state of the primary electron donor (P). Electron paramagnetic resonance spectroscopic (EPR) experiments on bacterial RCs showed that the photoinduced ET reaction originates from an electronically coupled special pair of bacteriochlorophyll (BChl) molecules that serve as the primary donor of electrons [4,5]. The strong electronic interaction between two closely positioned tetrapyrrole rings of BChl has been found to be characteristic of the primary electron donor structure in anoxygenic photosynthetic organisms [2,5,6]. Numerous experimental and theoretical investigations have been devoted to the characterization of the dimeric nature of the primary donor, the extent of electronic interactions between its counterparts, and interrelated electron transfer properties [7–11].

Structural details that emerged from crystallographic studies of RC protein complexes have substantially confirmed the overall models based on functional investigations, and have shown that not only the constituents of the primary donor special pair, but the entire protein core and associated cofactors are also doubled, forming two branches (Fig. 1). Besides the BChl molecules of the special pair (P_L and P_M), the central protein subunits L and M noncovalently bind two accessory BChls (B_L and B_M), two acceptor bacteriopheophytins (I_L and I_M), and two quinones (Q_L and Q_M). With the exception of the carotenoid cofactor, the L and M subunits are related by an approximate two-fold symmetry [12,13]. In the majority of bacterial photosynthetic organisms the RC has a bound cytochrome (Cyt). This tetraheme C subunit has its own internal local symmetry [14]. Even though the RC appears structurally balanced, functionally this protein complex is entirely asymmetrical. Light excitation of the primary donor to its lowest excited state P* initiates charge separation exclusively via cofactors associated

* Corresponding author.
E-mail address: Oleg@anl.gov (O.G. Poluektov).
[1] Current address: Chemical Sciences and Engineering Division, Argonne National Laboratory, 9700S, Cass Avenue, Argonne, IL 60439, USA.
[2] Current address: 444 Winthrop Place, Henderson, NV 89074, USA.

0005-2728/$ – see front matter. Published by Elsevier B.V.
doi:10.1016/j.bbabio.2010.06.002

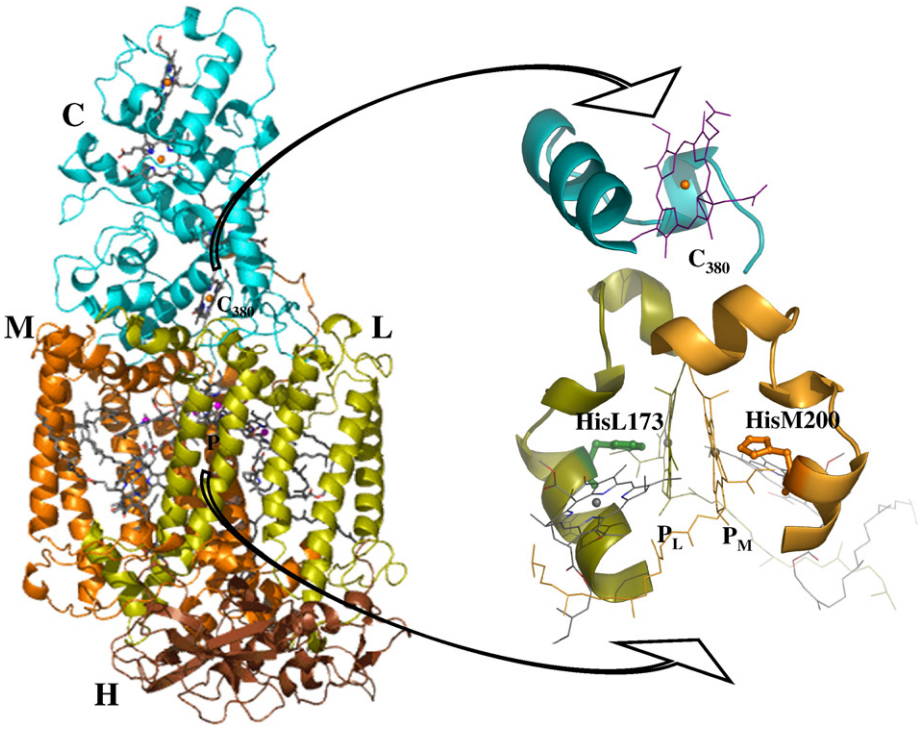

Fig. 1. Structure of the photosynthetic reaction center from *B. viridis*. The vicinity of primary electron donor with the closest heme C_{380} enlarged on the right. Sites of mutations, HisM200 and HisL173, are shown in "ball and stick" representation. Colors: orange – M subunit; green – L subunit; brown – H subunit; cyan – cytochrome C subunit.

with the L subunit. The symmetrically related cofactors located on the M side normally are photochemically nonfunctional [15,16].

As was shown by the analysis of paramagnetic states, this inequivalence starts from the electronic asymmetry of the primary donor [17,18], and is determined by differences in the dielectric environment of porphyrin cofactors. The surrounding protein matrix modulates conformations of the tetrapyrrole macrocycles along with the orientation of the substituent acetyl and carbonyl groups by providing electrostatic interactions with charged amino acids, hydrophobic interactions with aromatic or aliphatic amino acid residues, hydrogen bonding, and the essential magnesium coordination [12,13,19]. The central magnesium of the BChls in the RC is coordinated by four bonds from the tetrapyrrole ring and a histidine residue [12,13,20]. Residues HisL173 and HisM200 in *B. viridis* ligate to the BChls, P_L and P_M respectively, that represent each half of the special pair (Fig. 1). Mutation of His to Leu at either position causes the loss of the magnesium atom and the replacement of the corresponding BChl by bacteriopheophytin (BPhe) and, thus, these mutant RCs incorporate a BChl/BPhe heterodimer as the primary donor [21–23]. Since the oxidation potential of BPhe lies below that of BChl [24], significant changes in the properties of the heterodimer primary donor (D) occur as shown by EPR and other spectroscopic techniques [25–33].

Studies of the heterodimer mutants have greatly facilitated investigation of the primary donor electronic structure and have been important tests of both theoretical and experimental conclusions regarding the coupling of charge transfer states into the excitonically coupled dimer states [7,34–37]. These previous investigations were focused on two photosynthetic organisms possessing "minimal" variants of the RC that lack the tightly bound C subunit: *R. sphaeroides* and *R. capsulatus*. Because of the absence of intrinsic Cyt in these RCs, investigation of the next ET step following electron ejection from the primary donor, namely reduction of the oxidized special pair, requires introduction of an extraneous Cyt donor into the system [38,39]. This raises concerns about the docking ability of the cytochrome to mutated RCs, especially if the mutations affect the surface charge of RC or reduction potential of primary donor [40,41]. An alternative approach is to investigate this ET step in organisms possessing a bound cytochrome. In fact, a dominant number of anoxygenic bacterial organisms have RCs with permanently attached Cyt analogous to oxygenic photosynthetic apparatus [14,42]. Nevertheless, this approach has had serious experimental challenges as, even when Cyt containing strains were suitable for genetic alterations, no high resolution structure of the RC had been determined for those organisms. A clever solution for this problem was to combine two genomes. Thus, in [43,44] the expressed protein complex contained Cyt subunit originated from *B. viridis*, the organism with a crystallographically characterized RC, and core subunits derived from *Rubrivivax gelatinosus*, the strain capable of bearing mutations impairing the photosynthetic activity. Yet, this approach was only partially successful. Although the chimeric RC was able to function as a whole system, the natural conditions of photosynthetic ET were not reproduced because of shifted ratios between the reduction potentials of Cyt and primary donor.

The study of *B. viridis*, an organism having a well-characterized tetraheme Cyt as a forth subunit of the RC and a known high resolution crystal structure [45–48], has been limited by difficulties in the cultivation of mutant organisms that produce nonfunctional photosynthetic protein complexes. This constraint was overcome in the genetic system of Bylina et al. [49]. By application of this system, mutants with a loss of the histidine-coordinated magnesium of the primary donor from L or M side (His(L173)Leu and His(M200)Leu) were constructed in *B. viridis* and recently the crystal structure of the M heterodimer mutant RC has become available [50]. This allows one to test the effect of the internal asymmetry of wild type (WT) P^+ and heterodimer mutant primary donor D^+ states on re-reduction by the Cyt naturally present in the ET chain. Additionally, in view of the considerable asymmetry of the primary donor in *B. viridis* [34,51], the inequivalence of the heterodimer primary donor counterparts is likely more significant than corresponding heterodimers in *R. sphaeroides* and *R. capsulatus*. Thus the heterodimer status is expected to modify the normally dimeric primary donor of a bacterial photosynthetic organism into an almost monomeric primary donor, similar to the primary donor of photosystem II in oxygenic organisms [2,6].

This paper is focused on light-induced ET in *B. viridis* L and M heterodimer mutant RCs. High-frequency electron paramagnetic resonance (HF EPR) spectroscopy (D-band, 130 GHz, 4.6 T) has been used to analyze the primary donor electronic structure and the photoactivity in heterodimer His(M200)Leu and His(L173)Leu mutants compared to the homodimer of WT RCs. The superior spectral resolution of HF EPR allows for detailed characterization of the electronic state of donor and acceptor species as well as ET dynamics [52–54]. All experimental data indicate the monomeric electronic structure of the BChl/BPhe primary donor dimers in the RC mutants. EPR results demonstrate that a difference in the redox potential of the heterodimer primary donor constituents leads to a drop in ET efficiency and an alternation of ET pathways. At the same time, the enhancement of the semiquinone–iron pair EPR signals in the mutants indicates the presence of kinetically viable electron donors. HF EPR spectroscopy also resolved a BPhe anion radical formed within the heterodimer pair upon the photooxidation of mutant RCs. The important role of RC-bound Cyt in the formation of BPhe anion radical is discussed.

2. Experimental methods

2.1. Sample preparation

The H(M200)L and H(L173)L *B. viridis* reaction center mutants were constructed by oligonucleotide-directed mutagenesis [49,50]. Cells were grown semiaerobically under nonphotosynthetic conditions. The published procedure of reaction center protein complex purification [55] was modified by lowering the concentration of the detergent for membrane solubilization. Isolated RC complexes were suspended in 20 mM Tris–HCl buffer, pH 7.8, containing 1 mM ethylenediaminetetraacetic acid (EDTA) and 0.05% lauryldimethylamine oxide (LDAO). The RC concentrations were adjusted based on the accessory BChl absorbance peak at 832 nm as illustrated in Fig. 2. Based on the optical density of ca. 30 at this band and using the extinction coefficient of Clayton and Clayton [56], the RC concentrations in these experiments were estimated at 100 μM. WT RCs isolated from a deletion strain of *B. viridis* complemented with WT *puf* operon genes served as a reference system [49,50].

2.2. EPR measurements

X-band EPR spectra were recorded on a commercial Bruker ESP300E spectrometer equipped with a rectangular Bruker cavity and a variable temperature cryostat (Air Products) cooled to low temperatures by liquid helium. Temperature was regulated by an Oxford ITC503 temperature control system. Light excitation of the samples was achieved with a Xe 300 W lamp in combination with a 400 nm cutoff and a water filter. The standard modulation amplitude was 5 G and microwave power 2 or 10 mW. Samples were placed in quartz EPR tubes with an inner diameter of 3 mm.

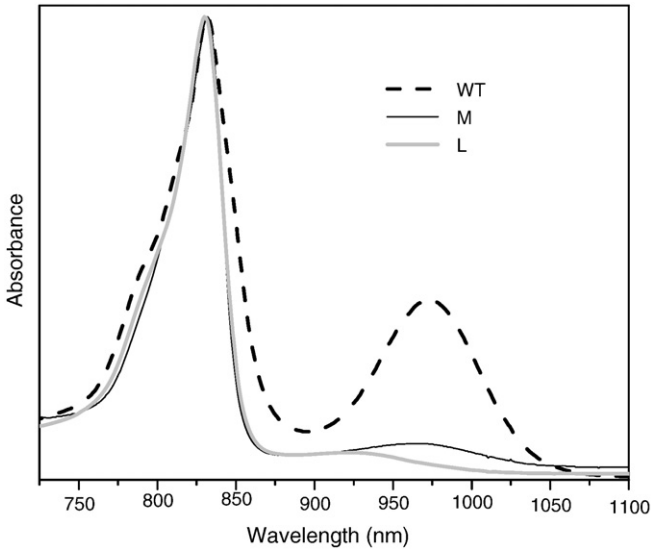

Fig. 2. Optical absorption spectra of RCs isolated from heterodimer mutants and WT strains. Dashed line – wild type; black – M mutant; grey bold – L mutant.

HF EPR spectra were recorded with a home-built continuous wave (CW)/pulsed D-band (130 GHz, 4.6 T) EPR spectrometer. The microwave bridge was developed by Dr. V. N. Krymov (HF EPR Instruments, Inc.) and consists of two independent channels driven by a frequency-fixed free running oscillator. Each channel has a linear IMPATT amplifier. Microwave power from each channel was combined by a 3 dB coupler and directed through the circulator to a single mode cylindrical TE_{011} cavity. The maximum power of the circulator output in the pulsed mode was 125 mW (which leads to 34 ns, π/2 pulses) and 3.4 mW in CW mode. The cylindrical cavity has several slits to allow for optical excitation and field modulation. Samples in quartz tubes with inner diameter of 0.5 mm and outer diameter of 0.6 mm were placed in the microwave cavity of the spectrometer. The sample temperature was regulated by an Oxford temperature controller (ITC 503) coupled to an Oxford continuous flow cryostat (CF 1200).

Light excitation of the samples was achieved in the cavity of the spectrometer with an optical parametric oscillator (Opotek) pumped by a Nd:YAG laser (Quantel). The output of the laser was coupled to fiber optics in order to deliver light to the cavity (1 mJ per pulse, 10 Hz repetition rate). The excitation wavelength was 550 nm. For accumulation of light-induced EPR signals P^+ and D^+, the RC samples were illuminated for ca. 1 min. at 10 K before the beginning of spectra acquisition. For recording EPR spectra of the RCs in their oxidized before illumination state, the samples were poised with the addition of 10 mM potassium ferricyanide (III) (concentration exceeded RC's by up to 100 times). For acquiring spectra of the RCs in pre-reduced, neutral before illumination state, 50 mM sodium ascorbate was added to the solutions (concentration exceeded RC's by ca. 500 times). The samples were dark-adapted at room temperature following the chemical treatment before freezing in the dark. Photoactivity was estimated by a change of the EPR signal intensity upon light excitation. EPR spectra were recorded by monitoring electron spin echo (ESE) intensity in two-pulse experiment as a function of magnetic field. The typical pulse sequence was 60 ns–200 ns–60 ns, and the repetition rate of the pulse sequence was 10 Hz. Light-induced spectra were represented as the difference spectra, accumulated under light influence or after it with subtraction of the spectrum recorded for the same dark-adapted sample prior to illumination.

The g-values were measured using Mn^{2+} impurities in a powder of MgO as a reference sample [57]. The MgO powder as an internal standard was glued on the surface of the plunger between the sample tube and the walls of the cylinder. As this experiment is very time-consuming, accurate g-value measurements were done only for several typical signals. Usually at HF EPR the accuracy in measuring absolute values of the g-tensor is low ($\sim 10^{-4}$), while a relative measurement is an order of magnitude higher. Unfortunately, in this case the deuteration of the mutants is not feasible and the canonical components of primary donors are not resolved. As a consequence the accuracy in the relative g-tensor measurements is also very low, and comparable with the accuracy of absolute g-values.

Triplet state spectra of the primary donor in mutants and WT RCs were detected using time-resolved ESE. Two microwave pulses followed a short 7 ns laser pulse with a fixed delay after laser flash (DAF) time. The triplet spectra were recorded similarly to stationary EPR spectra with a DAF time of 1 μs. High-field EPR spectra were simulated using the EasySpin the SimBad program [58], developed by Dr. A. Astashkin (The University of Arizona), and programs developed in our laboratory.

3. Results

3.1. Light-induced primary donor EPR signal

The activity of ET in the RC protein can be estimated with EPR spectroscopy by measuring the intensity of the light-induced cation radical signal of the primary donor. To compare the relative amounts of the primary donor cation radicals formed under illumination in the WT vs. mutant RCs (P^+ vs. D^+), EPR spectra were recorded using identical experimental parameters, excitation conditions and sample concentrations. An important difference observed in the amplitude of the signals of the heterodimer primary donor radicals is the apparent reduction in magnitude relative to the signal observed for WT, as evident from light-induced D-band EPR spectra (Fig. 3). Over 6 times decrease in amplitude of the mutant D^+ vs. the WT P^+ signal indicates a substantial decrease in the yield of the primary donor cation radical formation for the heterodimers. These results are analogous to X-band observations (Fig. S1). They are also consistent with the EPR signal intensity and shape of heterodimer primary electron donor signals observed for *R. capsulatus* and *R. sphaeroides* [25,30,59]. In both mutants, the EPR signal is broader than for WT (4.1 mT vs. 2.1 mT) and shifted to a lower magnetic field (Fig. 3). The signals increased with prolonged illumination and did not decay after the light was shut off.

3.2. Chemically oxidized RCs

To characterize in detail the primary donor electronic states, RCs were chemically oxidized with potassium ferricyanide. Under non-actinic conditions addition of potassium ferricyanide induced a dark EPR signal of the primary donor cation radical in WT RCs only. Following a short illumination period (~1 min) at low temperatures (10 K), the intensity of this WT signal increased. Upon light excitation, corresponding signals were formed in mutant organisms. The linewidth of these signals increases in the following order: WT, M mutant, L mutant and equals 2.1, 2.8, and 3.0 mT, respectively (see Fig. 4). In addition to changes in EPR linewidth, the mutant organisms RCs have peak positions (i.e., g-values) different from WT. Since the width and resonant field position of the EPR signals both depend on the strength of the coupling between the primary donor constituents [4,57], the shifts of the EPR signal in mutants toward lower fields, along with the increase in the linewidths, indicate a reduction of the internal electronic interaction between counterparts and enhancement of the electron localization on one half of the heterodimer primary donor. Based on these considerations and observations that the L mutant has the broadest EPR signal and the largest shift of its peak position, we can deduce that the coupling between the two porphyrin molecules of the donor is partially broken in the M mutant and almost completely destroyed in the L mutant. This conclusion is supported by the RC photoactivity, which is the weakest in the L mutant.

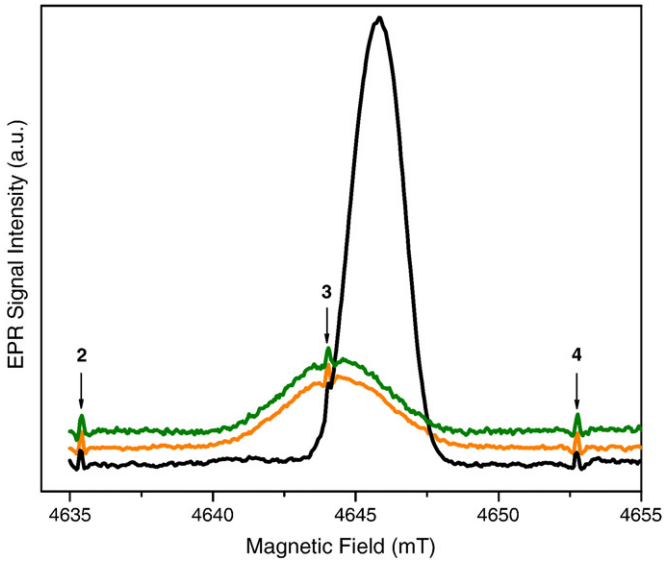

Fig. 3. ESE detected light-induced D-band (130 GHz, 4.6 T) HF EPR signals of primary donors in nontreated heterodimer mutants and WT recorded at $T = 10$ K. Black dashed line — WT; black — M mutant; grey bold — L mutant. Arrows show the positions of the three hyperfine lines (six in total) of Mn^{2+} impurities in a powder of MgO used as a g-value marker sample.

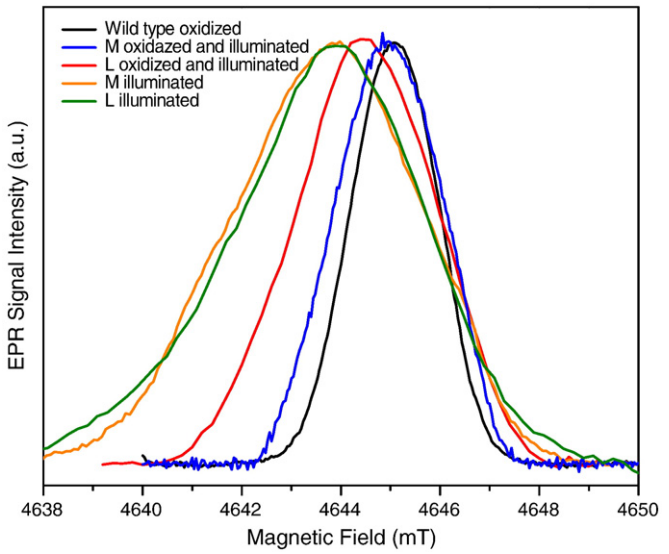

Fig. 4. ESE detected light-induced HF EPR signals of oxidized and untreated primary donors in mutant and WT RCs. Black – chemically oxidized WT, blue – chemically oxidized and illuminated M mutant, red – chemically oxidized and illuminated L mutant, orange – illuminated M mutant; olive – illuminated L mutant.

Comparison of the EPR signals induced by short light illumination (1 min) in untreated mutant samples versus chemically oxidized samples demonstrates the differences in their linewidths and positions (see Fig. 4). In order to clarify the nature of broad signals in untreated mutants we carry out the simulation of the EPR signals. Fig. 5 shows the HF EPR spectra of light illuminated WT RCs (identical to chemically oxidized RCs spectrum) and light illuminated untreated mutants (from Fig. 3) together with theoretical fits. As for the WT RCs, the spectrum is similar to the primary donor in purple photosynthetic bacteria and can be simulated with the following parameters: isotropic unresolved hyperfine interaction (hfi) of 10 G; $g_{xx} = 2.0032$; $g_{yy} = 2.0026$; $g_{zz} = 2.0021$. These parameters are in good agreement with previously reported data for the P^+ radical in *B. viridis* RCs [60]. The broad signal accumulated in the chemically untreated mutant RCs upon light illumination at low temperature can be simulated with the following set of parameters: hfi equals 16 G; $g_{xx} = 2.0044$; $g_{yy} = 2.0031$; $g_{zz} = 2.0020$. These g-tensors and, especially, the anisotropy of the g-tensor are similar to those reported for the intermediate bacteriopheophytin acceptor, I^- [61]. Based on the similarity of the magnetic resonance parameters and the considerations described in the discussion, we assign these signals to a BPhe anion radical. Importantly, we believe that this $BPhe^-$ signal is not that of the intermediate I^- acceptor, but rather that of the BPhe in the BChl/BPhe heterodimer primary donor. Note that the EPR signal of the reduced intermediate acceptor I_L^- can be detected in WT Fe-containing RCs where Q_L is doubly reduced [62,63]. In *B. viridis* WT, I^- photoaccumulates along with formation of the primary acceptor Q_L^-,, which is expected to be singularly reduced before I^- accumulation. Unpaired spins of I^-, Q_L^-, and Fe^{2+} are magnetically coupled and give rise to a characteristic broad split signal that is observed with X-band EPR at low temperature [62,64]. This signal cannot be observed at HF EPR due to the large width of the EPR line.

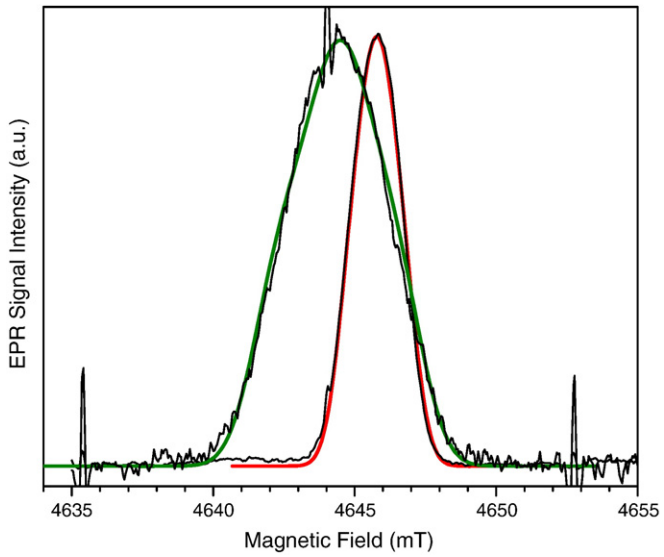

Fig. 5. ESE detected HF EPR signals of RCs shown in Fig. 3 and its theoretical fits. Light grey — theoretical simulation of primary donor spectrum in WT protein complex (overlapping with experimental spectrum — black dashed line); simulation parameters: $g_{xx}=2.0032$; $g_{yy}=2.0026$; $g_{zz}=2.0021$, isotropic unresolved hfi equals 10 G. Dark grey line — theoretical simulation of signal accumulated in the M mutant upon illumination (overlapping with experimental spectrum — black solid line; identical to L mutant signal); simulation parameters: $g_{xx}=2.0044$; $g_{yy}=2.0031$; $g_{zz}=2.0020$; hfi equals 16 G. Narrow signals at the edges and in the central part of the spectra are three hyprefine lines on Mn^{2+} in MgO, same as in Fig. 3.

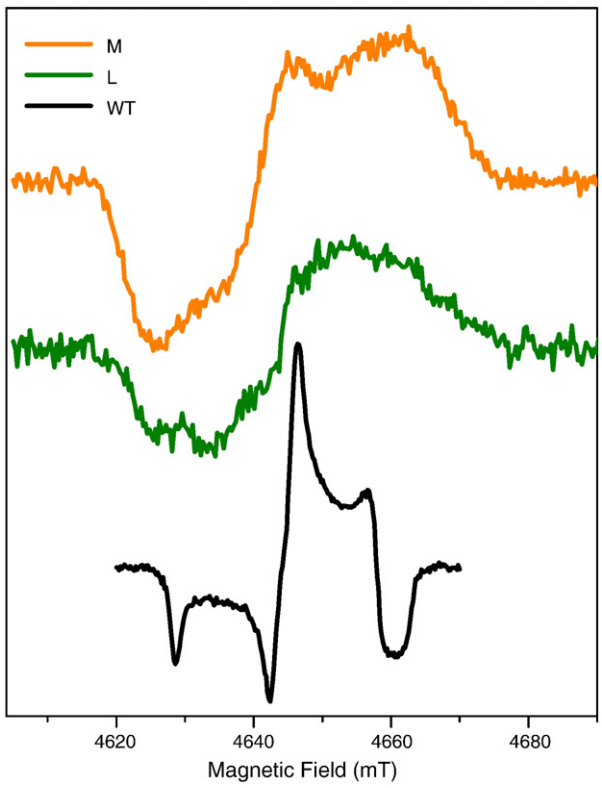

Fig. 6. ESE detected time-resolved HF EPR spectra (light minus dark) of triplet states in RCs recorded at 1 μs DAF time. Black dashed — WT; black solid — M mutant; grey bold — L mutant.

3.3. Chemically pre-reduced RCs

In RCs pre-reduced with sodium ascorbate, the HF EPR light-induced spectra were similar to chemically untreated RCs. In both pre-reduced mutant RCs, the effect of $BPhe^{-}$ radical anion accumulation under illumination is stronger than that observed for WT RCs. Moreover, in all reduced samples under prolonged illumination an additional signal with $g=2.0067$ at magnetic field 4636 mT is observed, identified as the ascorbyl radical (SD and Fig. S3).

3.4. HF EPR of triplet states in RCs

To further characterize the electronic properties of the donor-acceptor cofactors, time–resolved electron spin echo HF EPR spectra were obtained for RCs after chemical redox poising with sodium ascorbate, facilitating $D^{+}I_{L}^{-}$ radical pair accumulation and recombination required for the primary donor triplet state formation. Light-minus-dark time-resolved spectra recorded at 1 μs DAF time in mutant and WT RCs (Fig. 6) illustrate lineshapes typical of triplet state spectra of monomeric BChl and primary donors in photosynthetic RCs respectively [65].

In both mutants, the intensity of the triplet state signals were more than an order of magnitude smaller than in WT, indicating a reduction in triplet yield. A similar decrease in the intensity has been reported for heterodimer mutants of *R. capsulatus* [25] and *R. sphaeroides* [28,66] at X-band.

Theoretical simulations of the EPR lineshapes of these signals (Fig. 7) show that the zero-field splitting parameters for mutant RCs are $D=0.0224\ cm^{-1}$ and $E=0.0065\ cm^{-1}$, consistent values for monomeric BChl [65,67]. This is clear evidence that the triplet state is localized on a single BChl molecule in the M and L mutants, but delocalized over both BChl counterparts in the WT dimer ($D=0.0159\ cm^{-1}$ and $E=0.0040\ cm^{-1}$). For the primary donors having inequivalent counterparts in the heterodimer mutants of *R. capsulatus* and *R. sphaeroides*, localization of the triplet on the BChl half has been also shown by EPR [25,28,66] and ENDOR analyses [30,68].

3.5. Light-induced X-band EPR spectra

X-band EPR experiments were carried out to check light-induced electron transfer to Q_L. The X-band EPR spectra of RCs were recorded at 5 K. The difference spectra (after illumination minus before illumination) are shown in Fig. 9. During illumination the intensity of the signals in the $g=2.00$ region grows and then decays after termination of the light illumination, corresponding to light oxidation of the primary donor and to following charge recombination. However, the change in intensity of the primary donor signal due to the charge recombination is not completely reversible at low temperature. This residual signal is more intense in mutant organisms. The obvious changes are concomitant with the appearance of the signals around $g=1.82$ and $g=1.68$ (Fig. 8). As shown in earlier work [62,69], these signals are due to the Q_L^{-}, anion radical interacting with nearby high-spin nonheme Fe^{2+}. The semiquinone–iron radical pair lines are also more prominent in the mutants than in the WT. In order to prove that these signals at $g=1.82$ and $g=1.68$ belong to the $Q_L^{-}Fe^{2+}$ pair, we checked the power saturation and temperature dependence of these lines. Power saturation experiments provide evidence that these signals are related to a fast relaxing Fe^{2+} ion. They demonstrate that these signals are not saturated with an increase in microwave power, although the intensity of the P^{+} signal started to decrease (Fig. S4). Neither of these two signals is detectable at temperatures higher than 10K (Fig. S5). This allows us to identify $g=1.82$ and $g=1.68$ lines as the fast relaxing semiquinone–iron pair, $Q_L^{-}Fe^{2+}$. Accumulation of this radical pair provides direct evidence for light-induced ET to the L side quinone acceptor. The $Q_L^{-}Fe^{2+}$ radical could not be formed if the intermediate acceptor were in the reduced state I_L^{-} prior to (or during) illumination, as the electron would not be able to leave the excited primary donor. The reduced I_L^{-} acceptor can be trapped by illumination in the presence of a good electron donor to P^{+}, such as Cyt, but only after the preceding chemical reduction of Q_L

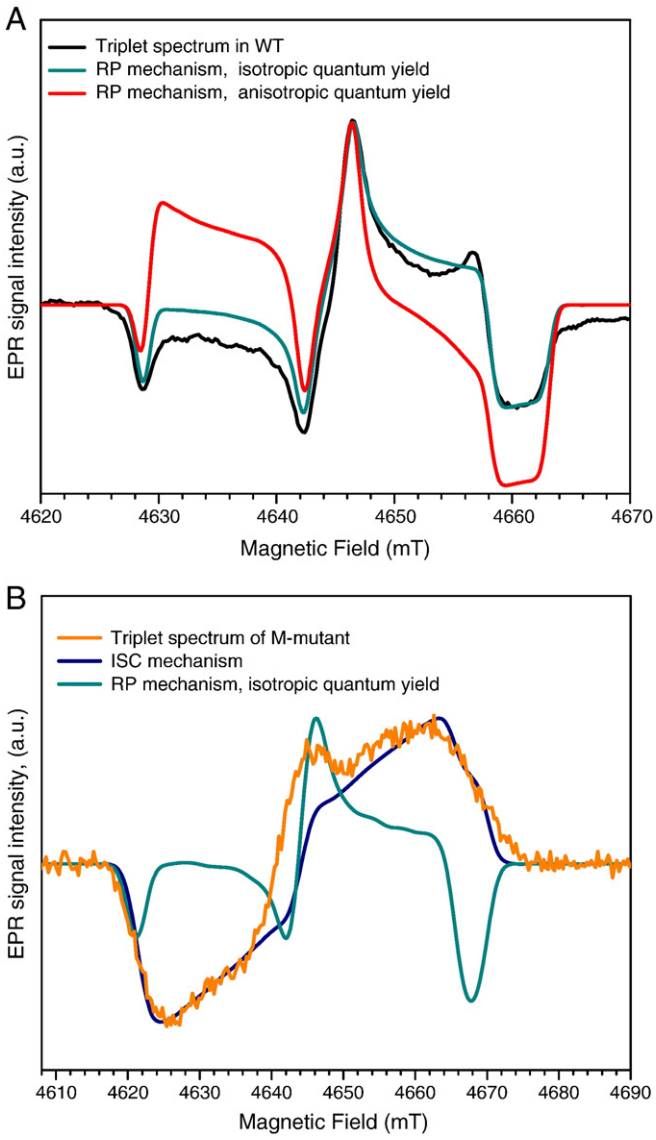

Fig. 7. Theoretical simulation of the EPR spectra of the primary donor triplet states. A — WT RCs. Black dashed — experimental spectrum; grey bold — radical pair mechanism; simulation parameters: only T_0 populated, isotropic quantum yield, zero-field splitting $D = 0.0159\ cm^{-1}$, $E = 0.0040\ cm^{-1}$, $g = (2.0036, 2.0031, 2.0023)$; light grey — radical pair mechanism; anisotropic quantum yield. B — M mutant RCs. Black solid — experimental spectrum; grey bold — ISC mechanism with simulation parameters: population rates $p_x = 0.5$, $p_y = 0.425$, $p_z = 0.075$, zero-field splitting $D = 0.0224\ cm^{-1}$, $E = 0.0065\ cm^{-1}$, isotropic unresolved hfi = 25 G; light grey — radical pair mechanism with isotropic quantum yield.

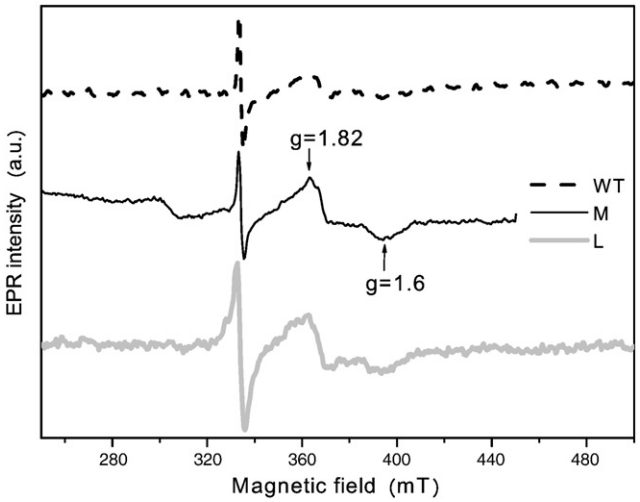

Fig. 8. X-band EPR signals in the RCs induced by light illumination. Depicted are the dark difference spectra: spectra acquired after illumination minus spectra recorded before illumination. $T = 4.7$ K, microwave power 10 mW. Dashed – WT; black – M mutant; grey bold – L mutant.

or its removal [5,62]. Furthermore, the characteristic shape of the reduced semiquinone–iron spectrum is quite different from the complex split signal which forms due to the magnetic interaction between reduced I_L acceptor and $Q_L^-Fe^{2+}$ [62,64]. In addition, along with the $Q_L^-Fe^{2+}$ radical pair, signals corresponding to the oxidized high potential hemes of Cyt were observed. The presence of these signals confirms Cyt is a donor in the ET pathway of heterodimer mutants.

The whole effect of residual signals can be explained by trapping part of the RCs in the charge-separated states ($C^+PI_LQ_L^-$,) in the WT and ($C^{2+}BChlBPhe^-I_LQ_L^-$,) in M or ($C^{2+}BPhe^-BChlI_LQ_L^-$,) in the L mutant. These trapped states would prevent the heterodimer mutants from further photoactivity. Thus, the intensity of the Q_L^-,Fe^{2+} signal is directly proportional to the trapped, charge-separated state and is inversely proportional to the remaining photoactivity of the RC. At ambient temperature the ET chain in *B. viridis* is extended owing to the secondary electron donor Cyt. However, at cryogenic temperature, the ET from the Cyt to the primary donor is significantly restricted in the native RCs of this organism [14,48,70,71]. The more efficient formation of the semiquinone–iron radical pair in heterodimer mutants is an indication of possible overcoming of the energetic constraints for primary donor reduction by Cyt imposed by cryogenic temperature in WT.

4. Discussion

Following photoexcitation of the primary donor in RCs, an electron is transferred from P through a series of intermediate acceptors to a primary quinone acceptor, forming a stabilized charge-separated state $P^+Q_L^-$. The observed intensity and reversibility of the light-induced P^+ EPR signal is an indicator of photoactivity of the RC. Heterodimer mutants have markedly decreased light-induced primary donor D^+ signal amplitudes compared to native RCs. This observation provides clear evidence of the reduced ET efficiency in donor-modified RCs, a consequence of the distortion of primary donor electronic structure in heterodimer mutants [72,73].

The primary donor special pair in native bacterial RCs is an electronically coupled dimer of bacteriochlorophyll molecules. In the oxidized state, the unpaired electron of the cation radical P^+ is highly delocalized over two BChl molecules, and the EPR spectrum exhibits a narrowing of the EPR linewidth relative to that of the BChl monomer due to averaging of the hyperfine interactions [4,18,74]. This delocalization is unequal in native RCs and is determined by differences in the dielectric environment of the two constituent BChls, P_L and P_M. Subtle structural modifications in the surrounding protein matrix result in an asymmetric electron-density distribution in the primary donor cation radical as well as in the excited state of the primary donor. This distribution conveys an elusive net charge transfer character ($P_L^+P_M^-$) to P^* which influences its intermolecular electronic interaction. Locally excited configurations $P_L^*P_M$ and $P_LP_M^*$bring in some contributions to the electronic structure of the primary donor excited state. These configurations combine some exciton character to the charge transfer configurations $P_L^+P_M^-$ and $P_L^-P_M^+$; the combination participates in the formation of the electronic asymmetry of $(P_LP_M)^*$ [16,75–78]. This asymmetry was traced by both experimental and theoretical investigations. The presence of significant charge transfer contribution to the excited singlet state of the primary donor was detected by optical spectroscopy [79,80]. The mixing of charge transfer states into the triplet wave function was invoked to explain the lower values of the zero-field splitting parameters of ^3P relative to the BChl monomer [51]. Molecular

orbital calculations by Plato et al. [8,81] have shown significant asymmetry of the orbital charge density distribution of the primary donor cation state with an excess of negative charge distribution on the P_M component of the dimer.

In heterodimer RCs, as a consequence of one BChl molecule being replaced by a BPhe, increased asymmetry of the primary donor is expected with more unpaired electron density localized on one half of the donor. This alteration should cause an increase in the observed EPR linewidth relative to the WT special pair [21,25]. Comparison of the linewidth of the light-induced EPR signals of oxidized primary donors in W-band confirmed the suggested broadening, indicating deviation of the primary donor radical cation from the dimeric state. At the same time, HF EPR spectroscopy reveals that the heterodimer primary donor radical signal induced by photochemical oxidation differs from the signal induced by illumination in nontreated and pre-reduced samples. Based on the theoretical fitting of these spectra (Fig. 5) we tentatively assigned the light-induced signals in untreated and pre-reduced mutants to a $BPhe^-$ that is not interacting with a semiquinone–iron pair, Q_L^-,Fe^{2+}. We propose that this $BPhe^-$ signal is a part of the primary donor in heterodimer RCs for the following reasons.

First, due to the difference in redox properties of BChl and BPhe molecules intrinsic to their electronic structures (in solution $E_m = -850$ mV vs. -550 mV) [24,82], the internal CT state would be more favored within the heterodimer special pair than in WT. BChl is a more efficient electron donor and tends to donate electrons initially to the BPhe constituent of the heterodimer. The anticipated intradimer charge transfer state in the M mutant excited primary donor is ($BChl_L^+BPhe_M^-$), with charge distribution similar to that of WT (Fig. 9). In the L heterodimer the intradimer electron donor component is converted into BPhe, which, based on its lower reduction potential relative to BChl, is the acceptor molecule. This is a prerequisite to the accumulation of the $BPhe_L^-BChl_M^+$ intradimer charge-separated state (Fig. 9). The existence of such a charge transfer state inside of the heterodimer primary donor has been shown in *R. capsulatus* and *R. sphaeroides* RCs when the photoinduced primary ET reactions were explored by ultrafast transient absorption spectroscopy [22,36,72,73]. The Fourier transform Raman investigation of the electronic structure and charge localization in the BChl/BPhe heterodimer from *R. sphaeroides* also revealed the presence of a charge transfer state with a dominant ($BChl^+BPhe^-$) configuration [31]. Data obtained by Stark spectroscopy also supported the view that the charge transfer state of the special pair is especially relevant to the analysis of ET in an asymmetrical primary donor [26,27]. Consequently, in the oxidized primary donor of both heterodimer mutants, the electronic unevenness of the constituent molecules accentuates localization of the remaining hole on the BChl molecule.

The degree of the energetic inequivalence of the two constituent molecules D_L and D_M of the heterodimer primary donor can be estimated with a Hückel molecular orbital model. This approach was successfully applied to the electronic structure analysis of the *R. sphaeroides* heterodimer RCs [83] and RCs with modified hydrogen bonding to the conjugated macrocycles of primary donor [19,84]. According to these studies, an increase in the primary donor midpoint potential correlates with the extent of asymmetry in the electronic structure of the dimer. A similar increase in midpoint potential of the heterodimer primary donor was expected in the *B. viridis* heterodimer mutants. Allowing for the higher asymmetry of the *B. viridis* primary donor relative to *R. sphaeroides*, an increase of E_m should be even more significant in the mutants of *B. viridis*. Therefore, we independently measured the midpoint potentials of D/D^+ in the *B. viridis* heterodimer mutant RCs [50] and confirmed that the midpoint potential is indeed higher than in the WT (772 mV in the M mutant versus 517 mV in the WT). The elevation is more significant than in *R. sphaeroides* (around 240 mV in *B. viridis* versus 160 mV in *R. sphaeroides* [85,86]). Taking into consideration the results of the EPR experiments described above, we conclude that in *B. viridis* the special pair has close to maximal asymmetry with very little electronic coupling between its counterparts. We speculate that in the highly asymmetric heterodimer supermolecule the loss of the interaction of its counterparts is so significant that in the oxidized primary donor the positively charged component is able to accept the electron autonomously. This is the second key reason for accumulation of intradimer BPhe-radical. Availability of an immediate source of electrons for the oxidized primary donor, tightly bound to RC Cyt, makes this possibility even more significant. Consequently the permanent presence of Cyt is the third important reason for the photo-accumulation of $BPhe^-$ within the heterodimer primary donor in *B. viridis*.

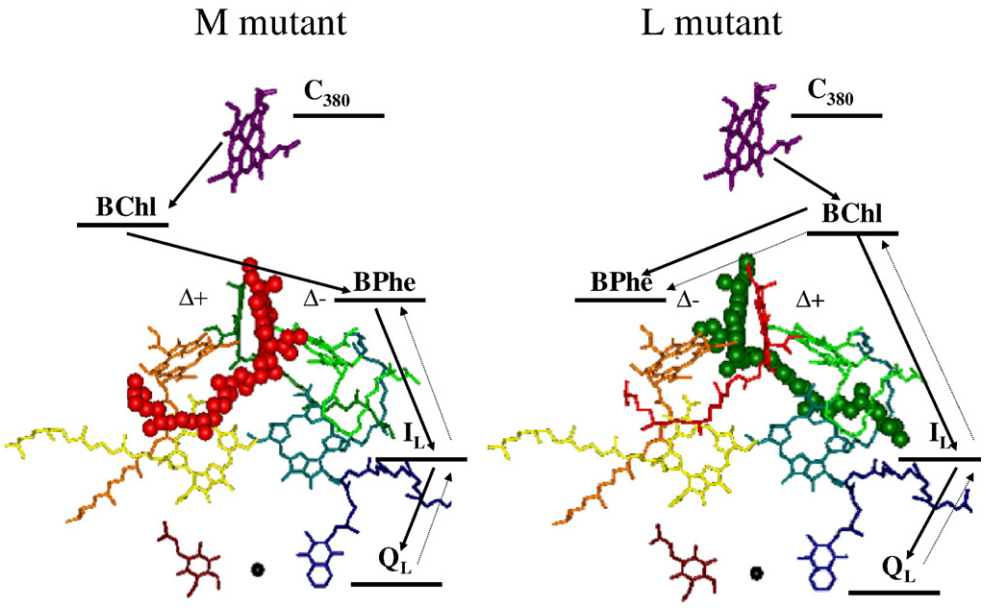

Fig. 9. Proposed scheme of the photoinduced reduction of BPhe counterpart of the heterodimer primary donor D. After the charge separation and formation of the $D^+Q_L^-$, radical pair, the hole is localized on $BChl_L$ in the M mutant (analogous to WT) or on $BChl_M$ in the L mutant. If Cyt reduced the $BChl^+$ half of the heterodimer primary donor before the $D^+Q_L^-$, radical pair recombination occurs, the returning electron from Q_L^-, will be localized on the $Bphe_M$ counterpart of primary donor immediately in M mutant and will be transferred to it via $BChl_M$ in L mutant in accordance to the difference in reduction potential of these molecules.

At ambient conditions, when usually only high potential hemes C_{380} and C_{320} are reduced in the Cyt of the WT RCs, reduction of P^+ by the Cyt dominates. At cryogenic temperature, ET from the Cyt to the photooxidized primary donor is constrained [14,48,70,71]. As shown by Frolov and others [87], the low-temperature limitations for the Cyt^-P^+ transition is caused by an energetic inhibition originating from an opposite shifting of the energy levels of the highest potential heme C_{380} and P^+. This is due to the freezing of protein dynamics and protein-bound water mobility. Because of competition between reduction by the Cyt and the charge recombination from Q_L^-, at cryogenic temperature, this reaction occurs at very slow rate; a number of reduced hemes in the bound Cyt are critical in determining at which temperature this reaction is still possible [47,64,87,88].

Low-temperature X-band EPR experiments verify light-initiated ET in the heterodimer mutant RCs and show the presence of a reduced Q_L^-, signal that is larger in amplitude than observed for WT RCs (Fig. 8). This enhancement of the semiquinone–iron pair EPR signals in the mutant RCs confirms that the electron donor D (Bchl/Bphe) is kinetically viable despite the substantially decreased relative amount of primary donor radical formation (cf. above). Based on the intensity of Q_L^-,Fe^{2+} signals, Cyt reduction of the heterodimer donor cation apparently dominates charge recombination from the semiquinone acceptor. The most straightforward explanation of the observed changes in EPR intensities found in mutants is the aforementioned increase of the heterodimer primary donor midpoint potential (by 255 mV in the M mutant [50]). This rise leads to a change in the relative E_m of the primary donor D/D^+ couple and the highest potential heme C_{380}/C_{380}^+ couple in the mutants and enhances oxidation of the Cyt hemes. Thus, the significant change in the driving force for ET from the Cyt, along with the alternation of hydrogen bond networks involved in redox-associated structural changes [23,50], might allow more dynamic oxidation of the Cyt at low temperature in the mutants. At analogous cryogenic conditions in RC mutants designed for the study of ET from the Cyt to the primary donor (with tyrosine L162 replaced by threonine or glycine), the low-temperature oxidation of a Cyt was maintained, leading to irreversible charge separation with a nearly temperature-independent reaction rate [47]. Though the reasons for analogous change of temperature behaviors are different, in both cases the fine-tuned ET sequence of the native organism, including the C_{380}/P^+ midpoint potential ratio, is altered by the introduced mutations.

Additionally, the change in the primary donor midpoint potential of heterodimer primary donor influences all related links of the ET chain. Since the rise of the redox potential was found to correlate with an increase in the rate of charge recombination from the primary quinone in *R. sphaeroides* [86], we can assume a similar effect in *B. viridis*. Thus, charge recombination from Q_L^-, together with (or in addition to) reduction by Cyt might result in the accumulation of an extra electron inside of the primary donor. This electron will reside on the BPhe molecule, which is the better electron acceptor half of the heterodimer (Fig. 9). Based on the reported cofactor redox potentials in organic solvents [24] and RCs we assume that in the M mutant the reduction potentials decrease in the sequence $BChl_L > BPhe_M > I_L > Q_L$. The extra electron resides on the active ET side. It does not have constraints for migration towards the intermediate and primary acceptors at ambient conditions, but at cryogenic temperatures it does have restrictions in charge recombination with the Cyt. Following the logic used for the M mutant, we presume that for the L mutant the Cyt reduces almost exclusively the BChl cation localized on the M side following electron transfer to Bphe in accordance with the reduction potentials of the two molecules. The sequence of the cofactor midpoint potentials is $BPhe_L < BChl_M > I_L > Q_L$. In this case, direct neutralization of the positive charge of the dimer, namely $BChl_M^+$, superimposed on the charge recombination from the primary acceptor, leads to trapping of the $Bphe_L^-$ anion and almost prevents participation of the primary donor L side in ET thereafter (Fig. 9). The detection of a $BPhe^-$ anion EPR signal uncoupled from semiquinone radical gives strong support to this hypothesis. Reduced intermediate BPhe and primary quinone acceptors would interact and produce the complex split signal $I_L^-Q_L^-Fe^{2+}$ due to the strong magnetic coupling [62,64]. Note that the amplitude of the $Q_L^-Fe^{2+}$ signal, as detected at X-band EPR, is at least twice higher in mutants relative to the WT. This is consistent with the presence of $BPhe^-$ inside the primary donor, since the potential barrier created by this anion prevents effective charge recombination.

Increasing the oxidation potential in systems with the addition of potassium ferricyanide caused the oxidation of the primary donor, along with Cyt, I, and Q only in the WT. Due to its elevated midpoint potential, the heterodimer primary donor remains neutral under these conditions and could be oxidized only in combination with illumination. Furthermore, all the hemes of the Cyt are oxidized, preventing any reduction by this internal electron donor. Thus, upon light illumination we were able to detect the primary donor cation radical with increased linewidth (Fig. 4), indicating the almost monomeric structure of the mutant's primary donor cation. By preventing reduction of the primary donor by the Cyt, the *B. viridis* heterodimer approximates RCs lacking bound Cyt, like *R. sphaeroides* and *R. capsulatus*, but with enhanced asymmetry. The evaluation at D-band allowed differentiation of this radical from $BPhe^-$ accumulated by illumination with participation of Cyt as instantaneous electron donor.

In the presence of sodium ascorbate as the external electron source for RCs the effect of accumulation of the $BPhe^-$ in the mutants is stronger, because almost all elements of the redox sequence, including the Cyt hemes, are reduced. This process is enhanced by the broadening of the redox gap between the actual E_h of the solution and the midpoint potential of the primary donor, already elevated in the mutants relative to the WT. Therefore, the driving force for the dimer reduction by the Cyt is increased, along with the higher rate of the charge recombination from the intermediate acceptor as Q_L is reduced by the chemical redox poising and the photoinduced charge separation. Similarly with the untreated RCs we can also assume that reduction of the BChl cation half of the primary donor after light-induced ET occurs concomitantly with production of the anion in the BPhe half of the donor.

Further evidence for asymmetry in the electronic structure of the heterodimer mutants primary donors comes from studying the triplet state by HF EPR. Since the localization of the triplet excitation explicitly depends on the electronic configuration of the primary donor, the triplet state magnetic parameters are therefore essential for the refinement of the electronic structure. The fundamental asymmetry of the primary donor was shown by an EPR measurement of the triplet state localization in the RC crystals [51]. These experiments gave an accurate estimation of the degree of its intradimer delocalization and also its dependence on the organism from which the RC is derived. In *B. viridis* the contribution of asymmetrical charge transfer configurations in the special pair triplet state is more significant than in *R. sphaeroides* [51]. This internal inequivalence was enhanced in heterodimer primary donors by introduced mutation, affecting the triplet state formation. The detected zero-field parameters of triplet state confirm its almost complete localization on a single molecule in the heterodimer primary donor. The considerably decreased intensity of the triplet state formation illustrate the recombination rate of the radical pair $D^+I_L^-$ is much higher for the heterodimer-containing RCs than for the WT RCs and is especially prominent in *B. viridis* (Figs. 6 and 7). The significance of this difference can be clarified by two mechanisms of triplet state formation in heterodimer mutants and WT primary donors. The first mechanism is the intersystem crossing (ISC). In this mechanism the triplet state of the molecule is formed after its excitation from the ground S_0 state into the first excited S_1 state, followed by further conversion to the energetically lower-lying triplet state T. The population of the triplet sublevels is determined by the spin-orbit

coupling between excited singlet state and triplet sublevels. The radical pair (RP) mechanism is the alternative pathway for triplet state formation. In this case, after the excitation of the donor P to the S_1 state, ET occurs to the acceptor molecule (in our case I), thus forming a radical pair in the singlet state $^1(P^+I^-)$. Due to singlet-triplet mixing, this RP can be transformed into a triplet radical pair $^3(P^+I^-)$ in which only the T_0 sublevel is populated. After back electron recombination from the $^3(P^+I^-)$ state, the T triplet state of the donor molecule is produced where only the T_0 sublevel is populated [51,65,67,89]. Theoretical simulation of the EPR lineshapes of the triplet states (Fig. 7) clearly shows that in the case of the WT RCs the triplet is formed by the RP mechanism, while in the case of mutants the ISC mechanism is effective. This indicates that in mutant organisms the ISC competes with ET in deactivation of excited state.

Thus, the drop in the photoinduced ET efficiency in the mutant RCs attributed to the altered charge delocalization within the special pair, confirms the extreme asymmetry in the electronic structure of the heterodimer primary electron donors.

In conclusion, using the high spectral resolution of HF EPR spectroscopy we investigated the electronic structure of the primary donor in heterodimer mutants of *B. viridis* reaction centers proteins. In these mutants amino acid substitutions His(M200)Leu or His(L173) Leu eliminate a ligand to the primary donor, resulting in the loss of magnesium in one of the constituent BChl and, as a consequence, conversion of the primary donor into the BChl/BPhe heterodimer.

Analysis of the HF EPR spectra of the photo-induced charge-separated states as well as triplet states in mutant and WT RCs confirms the hypothesis of the strongly asymmetric electronic structure of the heterodimer primary donors. The difference in the redox potential of the heterodimer primary donor constituents leads to the drop of the efficiency of the ET in mutant RCs and to the alteration of the ET pathways. Despite the substantial reduction in the primary donor radical formation, the enhancement of the EPR signals of the semiquinone–iron pair in the mutants indicates the presence of kinetically viable electron donors.

The formation of the stable $BPhe^-$ anion radical within the heterodimer primary donor accompanying photoinduced charge separation was observed in mutant RCs. Identification of the radical species as the $BPhe^-$ became possible owing to the high g-factor resolution of the HF EPR. The formation of $BPhe^-$ in mutants is facilitated by the presence of the Cyt subunit in the *B. viridis* which allows independent reduction of each constituent of heterodimer primary donor. The important role of cytochrome as a donor in the ET pathway of heterodimer mutants as well as ET kinetics will be discussed in a forthcoming publication.

Acknowledgements

N.S.P. would like to thank Dr. Richard Baxter for expert assistance in employing molecular structure visualization. The help of Dr. S. V. Pachtchenko in the simulation of HF EPR spectra is greatly appreciated. We gratefully acknowledge L. M. Rantala and L. M. Utschig for editing the manuscript. Work at University of Chicago was funded by the Division of Chemical Sciences, Geosciences, and Biosciences, Office of Basic Energy Sciences of the U.S. Department of Energy through Grant DEFG02-96ER14675. Work at ANL was supported by the Division of Chemical Sciences, Geosciences, and Biosciences, Office of Basic Energy Sciences of the U.S. Department of Energy through Grant DE-AC02-06CH11357.

Appendix A. Supplementary data

Supplementary data associated with this article can be found, in the online version, at doi:10.1016/j.bbabio.2010.06.002.

References

[1] R.E. Blankenship, Molecular mechanisms of photosynthesis, Blackwell Science, Oxford, 2002.
[2] G. Renger, in: G. Renger (Ed.), Primary processes of photosynthesis: principles and apparatus, Part 2, RSC Publishing, Cambridge, 2008, p. 327-290.
[3] J. Deisenhofer, J.R. Norris (Eds.), The photosynthetic reaction center, vol. 1-2, Academic Press, San Diego, CA, 1993.
[4] J.R. Norris, R.A. Uphaus, H.L. Crespi, J.J. Katz, Proc. Nat. Acad. Sci. U. S. A. 68 (1971) 625–628.
[5] G. Feher, J. Chem. Soc., Perkin Trans. 2 Phys. Org. Chem. (1972-1999) 11 (1992) 1861–1874.
[6] J. Barber, M.D. Archer, in: D. Mary, J.B. Archer (Eds.), Molecular to global photosynthesis, Imperial College Press, London, Singapore, River Edge, 2004, pp. 1–41.
[7] W.W. Parson, A. Warshel, J. Am. Chem. Soc. 109 (1987) 6152–6163.
[8] M. Plato, K. Moebius, M.E. Michel-Beyerle, M. Bixon, J. Jortner, J. Am. Chem. Soc. 110 (1988) 7279–7285.
[9] M.A. Thompson, M.C. Zerner, J. Fajer, J. Phys. Chem. 95 (1991) 5693–5700.
[10] J.R. Reimers, N.S. Hush, Chem. Phys. 197 (1995) 323–332.
[11] A.J. Hoff, J. Deisenhofer, Phys. Rep. 287 (1997) 1–247.
[12] U. Ermler, G. Fritzsch, S.K. Buchanan, H. Michel, Structure 2 (1994) 925–936.
[13] J. Deisenhofer, O. Epp, I. Sinning, H. Michel, J. Mol. Biol. 246 (1995) 429–457.
[14] W. Nitschke, S.M. Dracheva, in: R.E. Blankenship, M.M.T., C.E. Bauer (Eds.), Anoxigenic photosynthetic bacteria, Kluwer Academic Publishers, 1995, pp. 775–805.
[15] G.R. Fleming, J.L. Martin, J. Breton, Nature 333 (1988) 190–192.
[16] M.E. Michel-Beyerle, M. Plato, J. Deisenhofer, H. Michel, M. Bixon, J. Jortner, Biochim Biophys. Acta Bioenerg. 932 (1988) 52–70.
[17] J.R. Norris, C.P. Lin, D.E. Budil, J. Chem. Soc. Faraday Trans. 83 (1987) 13–27.
[18] J. Rautter, F. Lendzian, W. Lubitz, S. Wang, J.P. Allen, Biochemistry 33 (1994) 12077–12804.
[19] J.P. Allen, J.C. Williams, in: B. Grimm, W. Rudiger, R.J.P., H. Scheer (Eds.), Chlorophylls and bacteriochlorophylls: biochemistry, biophysics, functions and applications, Springer, 2006, pp. 283–295.
[20] J. Heimdal, K.P. Jensen, A. Devarajan, U. Ryde, J. Biol. Inorg. Chem. 12 (2007) 49–61.
[21] E.J. Bylina, D.C. Youvan, Proc. Nat. Acad. Sci. U. S. A. 85 (1988) 7226–7230.
[22] C. Kirmaier, E.J. Bylina, D.C. Youvan, D. Holten, Chem. Phys. Lett. 159 (1989) 251–257.
[23] A. Camara-Artigas, C. Magee, A. Goetsch, J.P. Allen, Photosynth. Res. 74 (2002) 87–93.
[24] J. Fajer, D.C. Brune, M.S. Davis, A. Forman, L.D. Spaulding, Proc. Natl. Acad. Sci. U. S. A. 72 (1975) 4956–4960.
[25] E.J. Bylina, S.V. Kolaczkowski, J.R. Norris, D.C. Youvan, Biochemistry 29 (1990) 6203–6210.
[26] S.L. Hammes, L. Mazzola, S.G. Boxer, D.F. Gaul, C.C. Schenck, Proc. Natl. Acad. Sci. U. S. A. 87 (1990) 5682–5686.
[27] T.J. DiMagno, E.J. Bylina, A. Angerhofer, D.C. Youvan, J.R. Norris, H. Scheer, J.J. Katz, Biochemistry 29 (1990) 899–907.
[28] H.A. Frank, J. Innes, M. Aldema, R. Neumann, C.C. Schenck, Photosynth. Res. 38 (1993) 99–109.
[29] M. Huber, J.T. Tarring, Chem. Phys. 194 (1995) 379–385.
[30] M. Huber, R.A. Isaacson, E.C. Abresch, D. Gaul, C.C. Schenck, G. Feher, Biochim. Biophys. Acta 1273 (1996) 108–128.
[31] D. Albouy, M. Kuhn, J.C. Williams, J.P. Allen, W. Lubitz, T.A. Mattioli, Biochim. Biophys. Acta Bioenerg. 1321 (1997) 137–148.
[32] E. Nabedryk, C. Schulz, F. Muh, W. Lubitz, J. Breton, Photochem. Photobiol. 71 (2000) 582–588.
[33] M.E. Brederode, I.H.M. Stokkum, E. Katilius, F. Mourik, M.R. Jones, R. Grondelle, Biochemistry 38 (1999) 7545–7555.
[34] M. Plato, F. Lendzian, W. Lubitz, K. Moebius, NATO ASI Ser., Ser. A (Photosynthetic Bacterial Reaction Center II) 237 (1992) 109–118.
[35] J.M. Hughes, M.C. Hutter, J.R. Reimers, N.S. Hush, J. Am. Chem. Soc. 123 (2001) 8550–8563.
[36] C. Kirmaier, J.A. Bautista, P.D. Laible, D.K. Hanson, D. Holten, J. Phys. Chem. B 109 (2005) 24160–24172.
[37] W.W. Parson, Compre. Ser. Photochem. Photobiol. Sci. (Prim. Process. Photosynth. 2) 57 (2008) 59–109.
[38] H.L. Axelrod, E.C. Abresch, M.Y. Okamura, A.P. Yeh, D.C. Rees, G. Feher, J. Mol. Biol. 319 (2002) 501–515.
[39] O. Miyashita, M.Y. Okamura, J.N. Onuchic, Proc. Natl. Acad. Sci. U. S. A. 102 (2005) 3558–3563.
[40] J. Wachtveitl, J.W. Farchaus, P. Mathis, D. Oesterhelt, Biochemistry 32 (1993) 10894–10904.
[41] X. Lin, J.C. Williams, J.P. Allen Test, Biochemistry 33 (1994) 13517–13523.
[42] T. Nogi, Y. Hirano, K. Miki, Photosynth. Res. 85 (2005) 87–99.
[43] H. Maki, K. Matsuura, K. Shimada, K.V.P. Nagashima, J. Biol. Chem. 278 (2003) 3921–3928.
[44] J. Alric, J. Lavergne, F. Rappaport, A. Vermeglio, K. Matsuura, K. Shimada, K.V.P. Nagashima, J. Am. Chem. Soc. 128 (2006) 4136–4145.
[45] O. Kaminskaya, P.J. Bratt, M.C.W. Evans, Chem. Phys. 194 (1995) 335–548.
[46] E. Nabedryk, C. Berthomieu, A. Vermeglio, J. Breton, FEBS Lett. 293 (1991) 53–58.
[47] J.M. Ortega, B. Dohse, D. Oesterhelt, P. Mathis, Biophys. J. 74 (1998) 1135–1148.
[48] J.M. Ortega, F. Drepper, P. Mathis, Photosynth. Res. 55 (1998) 337–341.
[49] E.J. Bylina, K.A. Ohgi, T. Nute, S. O'Neal, P. Weaver, Biotechnol. et alia (2002) 1–23.

[50] N.S. Ponomarenko, L. Li, A.R. Marino, V. Tereshko, A. Ostafin, J.A. Popova, E.J. Bylina, R.F. Ismagilov, J.R.J. Norris, Biochim. Biophys. Acta Biomembr. 1788 (2009) 1827–1831.
[51] J.R. Norris, D.E. Budil, P. Gast, C.-H. Chang, O. El-Kabbani, M. Schiffer, Proc. Natl. Acad. Sci. U. S. A. 86 (1989) 4335–4339.
[52] S. Un, P. Dorlet, A.W. Rutherford, Appl. Magn. Reson. 21 (2001) 341–361.
[53] K. Mobius, A. Savitsky, M. Fuchs, Biological magnetic resonance 22 (very high frequency (VHF) ESR/EPR), 2004, pp. 45–93.
[54] M. Bennati, T.F. Prisner, Rep. Prog. Phys. 68 (2005) 411–448.
[55] G. Fritzsch, Meth. Enzymol. 297 (1998) 57–77.
[56] R.K. Clayton, B.J. Clayton, Biochim. Biophys. Acta 501 (1978) 478–487.
[57] O.G. Poluektov, L.M. Utschig, S.L. Schlesselman, K.V. Lakshmi, G.W. Brudvig, G. Kothe, M.C. Thurnauer, J. Phys. Chem. B 106 (2002) 8911–8916.
[58] S. Stoll, A. Schweiger, J. Magn. Reson. 178 (2006) 42–55.
[59] M. Huber, J.T. Tarring, M. Plato, U. Finck, W. Lubitz, R. Feick, C.C. Schneck, K. Mobius, Sol. Energy Mater. Sol. Cells 38 (1995) 119–126.
[60] P.J. Bratt, P. Heathcote, A. Hassan, J. van Tol, L.-C. Brunel, J. Schrier, A. Angerhofer, Chem. Phys. 294 (2003) 277–284.
[61] P. Dorlet, A.W. Rutherford, S. Un, Biochemistry 39 (2000) 7826–7834.
[62] R.C. Prince, D.M. Tiede, J. Thornber, P. Dutton, P. Leslie, Biochim. Biophys. Acta 462 (1977) 467–490.
[63] G. Feher, M.Y. Okamura, Appl. Magn. Reson. 16 (1999) 63–100.
[64] J.S. Van den Brink, P. Gast, A.J. Hoff, J. Chem. Phys. 104 (1996) 1805–1812.
[65] D.E. Budil, M.C. Thurnauer, Biochim. Biophys. Acta Bioenerg. 1057 (1991) 1–41.
[66] J. Vrieze, C.C. Schenck, A.J. Hoff, Biochim. Biophys. Acta Bioenerg. 1276 (1996) 229–238.
[67] T.L. Trosper, H.A. Frank, J.R. Norris, M.C. Thurnauer, Biochim. Biophys. Acta Bioenerg. 679 (1982) 44–50.
[68] M. Huber, Photosynth. Res. 52 (1997) 1–26.
[69] W. Lubitz, G. Feher, Appl. Magn. Reson. 17 (1999) 1–48.
[70] J.-L. Gao, R.J. Shopes, C.A. Wraight, Biochim. Biophys. Acta Bioenerg. 1015 (1990) 96–108.
[71] J.M. Ortega, P. Mathis, FEBS Lett. 301 (1992) 45–48.
[72] L.M. McDowell, D. Gaul, C. Kirmaier, D. Holten, C. Schenck, Biochemistry 30 (1991) 8315–8322.
[73] M.E. Van Brederode, I.H.M. van Stokkum, E. Katilius, F. van Mourik, M.R. Jones, R. van Grondelle, Biochemistry 38 (1999) 7545–7555.
[74] F. Lendzian, M. Huber, R.A. Isaacson, B. Endeward, M. Plato, B. Boenigk, K. Moebius, W. Lubitz, Biochim. Biophys. Acta Bioenerg. 1183 (1993) 139–160.
[75] P.O.J. Scherer, S.F. Fischer, Chem. Phys. 131 (1989) 115–127.
[76] P.O.J. Scherer, S.F. Fischer, Spectrochim. Acta Part A 54A (1998) 1191–1199.
[77] E.J.P. Lathrop, R.A. Friesner, J. Phys. Chem. 98 (1994) 3056–3066.
[78] M.R. Gunner, A. Nicholls, B. Honig, J. Phys. Chem. 100 (1996) 4277–4291.
[79] M. Losche, G. Feher, M.Y. Okamura, Proc. Natl. Acad. Sci. U. S. A. 84 (1987) 7537–7541.
[80] L.J. Moore, H. Zhou, S.G. Boxer, Biochemistry 38 (1999) (1960) 11949–11960.
[81] M. Plato, W. Lubitz, F. Lendzian, K. Moebius, Isr. J. Chem. 28 (1988) 109–119.
[82] M.S. Davis, A. Forman, L.K. Hanson, J.P. Thornber, J. Fajer, J. Phys. Chem. 83 (1979) 3325–3333.
[83] K. Artz, J.C. Williams, J.P. Allen, F. Lendzian, J. Rautter, W. Lubitz, Proc. Natl. Acad. Sci. U. S. A. 94 (1997) 13582–13587.
[84] A. Ivancich, K. Artz, J.C. Williams, J.P. Allen, T.A. Mattioli, Biochemistry 37 (1998) (1820) 11812–11820.
[85] D. Davis, A. Dong, W.S. Caughey, C.C. Schenck, Biophys. J. 61 (1992) A153(abstr).
[86] J.P. Allen, K. Artz, X. Lin, J.C. Williams, A. Ivancich, D. Albouym, T.A. Mattioli, A. Fetsch, M. Kuhn, W. Lubitz, Biochemistry 35 (1996) 6612–6619.
[87] E.N. Frolov, V.I. Goldanskii, A. Birk, F. Parak, Eur. Biophys. J. 24 (1996) 433–438.
[88] W. Nitschke, A.W. Rutherford, Biochemistry 28 (1989) 3161–3168.
[89] M. Volk, A. Ogrodnik, M.-E. Michel-Beyerle, in: R.E. Blankenship, M.M.T., C.E. Bauer (Eds.), Anoxygenic photosynthetic bacteria, 1995, pp. 595–626.